Microsyst Technol (2009) 15:973–979
DOI 10.1007/s00542-009-0823-4

TECHNICAL PAPER

# Resonant frequency sensitive MEMS bandpass filter using capacitive sensing scheme

**In-Hyouk Song · Yves-Alain Peter · Michel Meunier**

Received: 13 November 2008 / Accepted: 13 March 2009 / Published online: 31 March 2009


**Abstract** This paper presents the theoretical and experimental behaviour of microelectromechanical bandpass filters. The proposed bandpass filter can detect frequencies of monitoring structures with high sensitivity using the resonant frequency of micro-resonator of sensor. The micro-resonator contains a proof mass and four supported beams fabricated using a bulk silicon micromachining technology on a silicon-on-insulator wafer. When applying an external force to the system, the device generates a capacitance change, which is converted into a voltage by an electrical circuitry. In good agreement with finite element simulations of the device, experimental results validate that the filter has a center frequency of about 3.3 kHz, a 3 dB bandwidth of 0.562 kHz and a quality factor $Q$ of 5.9 in atmospheric pressure. This paper demonstrates a parallel-resonator filter to increase a monitoring bandwidth. A 3 dB bandwidth of the parallel filter is measured to be 1.25 kHz at atmospheric pressure.

I.-H. Song (✉) · Y.-A. Peter · M. Meunier
Department of Physics Engineering,
École Polytechnique de Montréal,
Montréal, QC, Canada H3C 3A7
e-mail: in-hyouk.song@polymtl.ca

Y.-A. Peter
e-mail: yves-alain.peter@polymtl.ca

M. Meunier
e-mail: michel.meunier@polymtl.ca

## 1 Introduction

Recently, microelectromechanical systems (MEMS) have been seriously considered as a candidate for sensor applications since it affords an opportunity for simultaneous signal amplification along with its detection to improve the measured signal to noise ratio. Due to the utilization of existing IC standards, MEMS techniques offer low cost mass production with a high degree of uniformity. MEMS sensors have been investigated with a variety of transduction mechanisms such as piezoresistive, capacitive and other sensing schemes (Seidel et al. 1995; Reithmuller et al. 1992; Ludtke et al. 2000; Yeh and Najafi 1997; Song and Ajmera 2009; Li et al. 2001).

In this paper, we propose a resonant frequency sensitive MEMS bandpass filter using capacitive sensing scheme. The bandpass filter is used in a variety of applications such as communication system, navigation equipment and system control. Specially, mechanical filters are used for a good stability, low loss and narrow band selective systems (Johnson 1983). The bandpass filter is required to attenuate or reduce signals with frequencies outside passband, while passing signals within band. The proposed MEMS bandpass filter in this paper uses a resonant frequency of micro-resonator as an operating frequency or a passband. It is useful to monitor an input frequency with a small actuation force. Since the proposed device works at its own resonant frequency, the signal to noise ratio is improved by high quality factor. It provides both high selectivity and sensitivity since the displacement of moving structure is maximized at resonant frequency for a given force or acceleration.

This paper discusses experimental data obtained from micro-resonators consisting of a proof mass and serpentine springs. Section 2 serves to introduce the designed device

and its electrical and mechanical simulation. Section 3 discusses the fabrication details of the devices. The experimental results are presented and discussed in Sect. 4.

## 2 Design and simulation

The bandpass filter working at resonant frequency enhances device sensitivity and selectivity. The sensing principle is based on the displacement of a proof mass from its rest position which affects the capacitance between the proof mass and a fixed conductive electrode separated from it with a narrow gap. A mechanical design of the micro-resonator is shown in Fig. 1. The capacitance is formed between the movable fingers and the fixed ones parallel to them. The sensing direction for the resonator is in the $x$-direction of Fig. 1.

### 2.1 Design and dynamic consideration

Each dimension and shape is carefully designed to account for fabrication and operation. The moving and spring structure material is single crystal silicon to eliminate residual stress in the structures. The thickness of the moving structure is 80 μm. The resonator consists of a planar proof mass with comb fingers to increase sensing area efficiency and to sense the relative displacement between the proof mass and the fixed outer electrode.

The inertial sensor can be expressed as a lumped model consisting of a proof mass $M$ suspended by compliant beams anchored to a rigid fixed frame, where the suspended beams work as springs with effective spring constant $K$. There is a damping coefficient $D$ which affects the dynamic response of the proof mass. Time dependant external force $F(t)$ such as acceleration induces displacement of proof mass from its rest position. The oscillation mode can be described by a second order differential equation of motion:

$$F(t) = Kx + D\frac{\partial x}{\partial t} + M\frac{\partial^2 x}{\partial t^2}, \tag{1}$$

where $x$ is the absolute displacement of the proof mass. For the case of sinusoidal oscillations with constant amplitude $F_0$ and frequency $\omega$, the amplitude of displacement $X$ is expressed as

$$X = \frac{F_0}{\sqrt{(K - M\omega^2)^2 + (D\omega)^2}}. \tag{2}$$

The ratio of dynamic displacement $X$ to a static displacement ($X_0 = F_0/K$) is given by

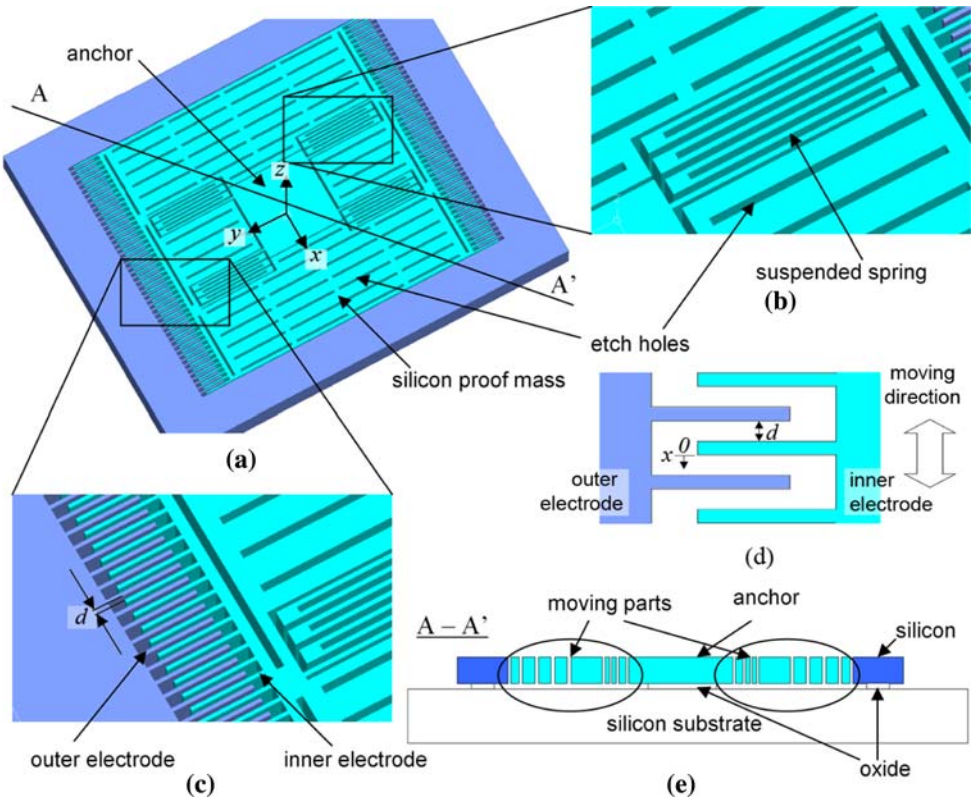


**Fig. 1** **a** Schematic diagram of the micro-resonator using capacitive sensing scheme. **b** Close-up view of the retaining spring structure. **c** Close-up view of the sensing electrodes. $d$ is the gap between outer electrode and inner electrode. **d** Close-up view of the sensing electrodes. $x$ is the moving distance of inner electrode. **e** Cross-section view of A–A′ in Fig. 1a

$$\frac{X}{X_0} = \frac{1}{\sqrt{\left(1 - \frac{\omega^2}{\omega_n^2}\right)^2 + \left(2\zeta\frac{\omega}{\omega_n}\right)^2}}, \tag{3}$$

where $\omega_n$ is the undamped resonant frequency. $\zeta$ is a damping ratio of the system given by

$$\zeta = \frac{D}{2\sqrt{K \cdot M}}. \tag{4}$$

As shown in (3), the motion is maximized when the input frequency $\omega$ is equal to the resonant frequency $\omega_n$. In contrast, for the motion with the frequency far from resonant frequency, the displacement is much smaller than that at the resonant frequency. Hence, the advantage of MEMS bandpass filter using a resonant frequency sensitive sensing scheme is to filter out the unwanted signal. It is very useful to apply this device for vibration based SHM applications.

### 2.2 Simulations

As shown in Fig. 1, four meander type springs support the moving plate. In order to determine the resonant frequency of the structure, the suspended mass structure and the supported beam stiffness should be optimized. In a one-axis sensing device, the proof mass must be displaced in the same direction as the sensing direction at the first resonant frequency. The square in the center of the proof mass is the anchor that fixes the moving structure to the substrate.

Finite element method (FEM) simulations with ANSYS have been performed. A solution of the analyzed FEM model for a static acceleration is shown in Fig. 2. According to the simulation, the first resonant frequency occurs at 3.3 kHz in the $x$-direction, the second mode is rotating around the $z$-direction at 3.7 kHz, and the structure is oscillating in the $y$-direction at 8.6 kHz at the third mode.

Since the system does not use electrostatic force, the electrical short problem between inner electrode and outer electrode is not considered. The gap $d$ along the sensing direction of a comb-finger is limited by the performance of dry etching for high-aspect-ratio structures and has been fixed at 5 μm. The initial capacitance $C_0$ at rest state is given as

$$C_0 = \frac{\varepsilon_0 A}{d}, \tag{5}$$

where $\varepsilon_0$ is the free-space permittivity and $A$ is the total electrode area of capacitor. The initial capacitance of the designed structure is of 1.927 pF. Since the design utilizes a single mode capacitance and inner electrode comb fingers

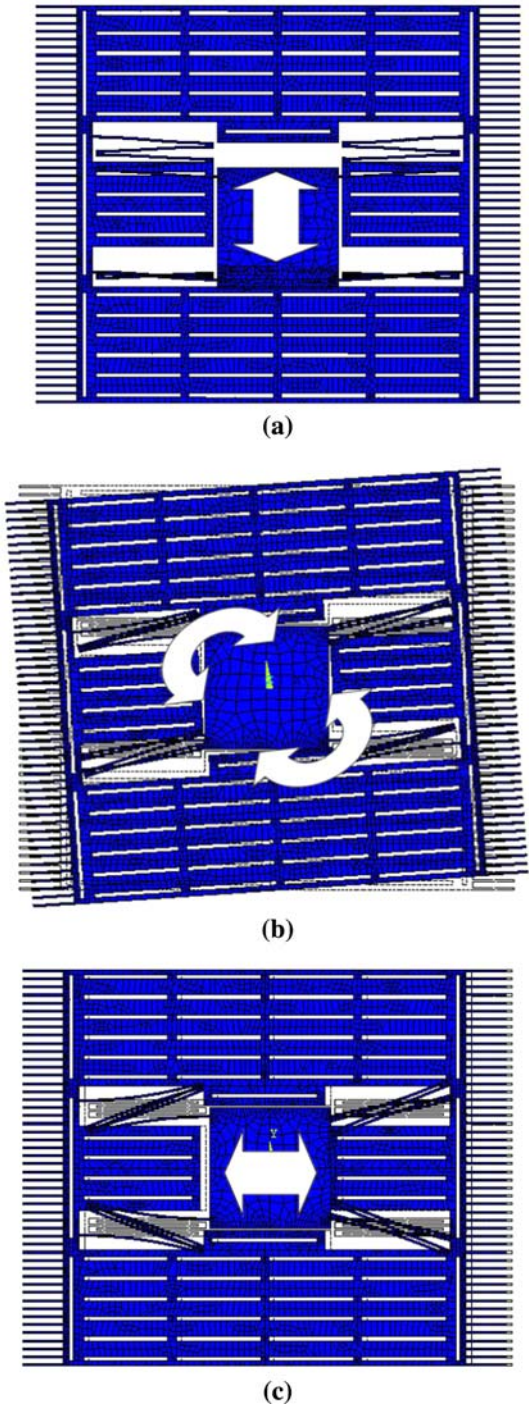


**Fig. 2** The first three resonant modes simulated by FEM. **a** First mode: 3.3 kHz. **b** Second mode: 3.7 kHz. **c** Third mode: 8.6 kHz

are located at the middle of gaps of outer electrode fingers, the value of capacitance always increases upon any displacement from its rest position. Thus, the change in capacitance $\Delta C$ is due to the displacement of the moving plate $x$ and is given by

$$\Delta C = \frac{\varepsilon_0 A}{2}\left\{\frac{1}{(d-x)} + \frac{1}{(d+x)}\right\} - C_0. \quad (6)$$

As shown in (6), the capacitance response is quadratic in the displacement. It is beneficial to eliminate small signals including noises and improve the sensitivity of the device. Figure 3 illustrates $\Delta C$ as a function of the displacement $x$. For example, for $x = 3$ μm, the capacitance is shifted by 1.084 pF from the initial capacitance while for $x < 1$ μm, the change in capacitance shows less than 0.08 pF. Substituting (2) into (6) leads to the capacitance change as a function of frequency.

## 3 Fabrication

The micro-resonator is fabricated using a bulk silicon micromachining technology on a silicon-on-insulator (SOI) wafer. The device layer is 80 μm thick highly doped p-type (100) Si. The device layer and the handle layer are separated by a 3 μm thick oxide layer which is used here as a sacrificial layer. A one-mask process illustrated in Fig. 4 is used to structure the micro-resonator.

First, a 7 μm thick SPR 220 photoresist is spin-coated on the device layer as a mask layer for deep reactive ion etching (DRIE) Bosch process. It is then patterned with UV-lithography, thus creating opening windows for Si etching (Fig. 4a). The opened Si areas are etched down to the oxide layer by the DRIE process (Fig. 4b), which is useful to realize vertical sidewall microstructures with a relatively high etch rate. The DRIE Bosch process is based on alternating Si etching steps using $SF_6$ as reacting gas and passivation steps by fluorocarbon polymer layer deposition from $C_4F_8$. The formed passivation layer during the DRIE Bosch process and the photoresist mask layer are simultaneously stripped away by an $O_2$ plasma etching process. The sacrificial oxide layer underneath the moving structure is selectively etched out using a HF vapour phase oxide etching method, which is suitable to release moving parts without leaving any stiction (Fig. 4c). Figure 5 shows an SEM picture of the fabricated micro-resonator.

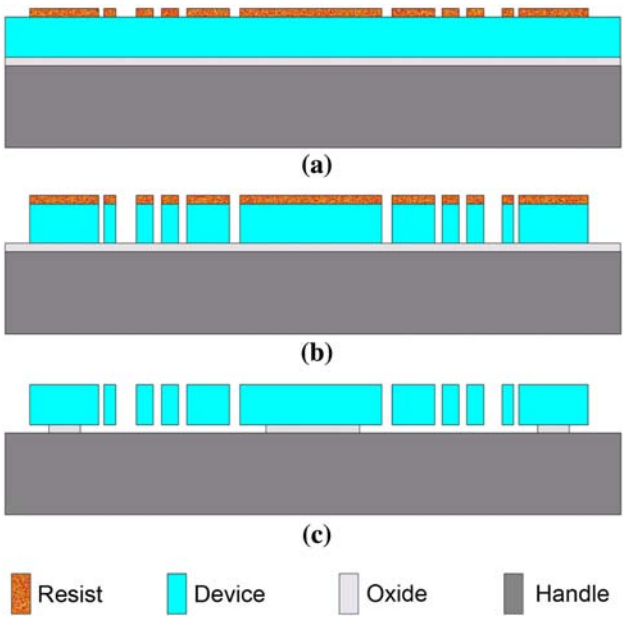


**Fig. 4** Schematic diagrams of the fabrication procedure using deep reactive ion etching (DRIE) technique on SOI wafer. **a** 7 μm thick SPR 220 photoresist mask patterning using UV-lithography. **b** 80 μm deep Si-device layer etching using the DRIE Bosch process. **c** Sacrificial oxide layer etching to release moving parts using HF vapour phase etching method

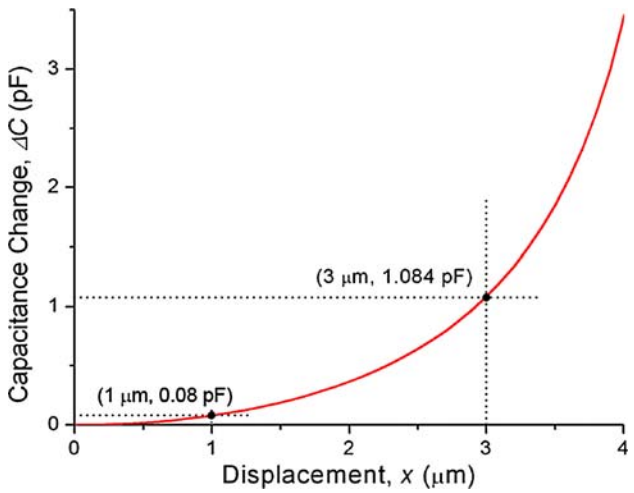


**Fig. 3** Capacitance change versus the moving electrode displacement

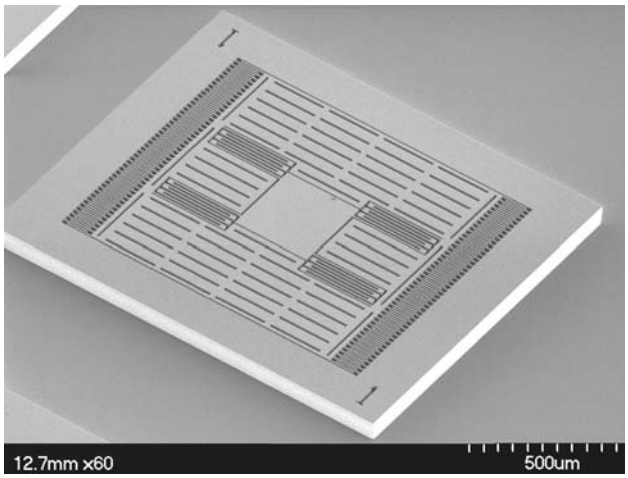


**Fig. 5** SEM photograph of the fabricated micro-resonator after sacrificial layer etching

## 4 Device characterization

The distance variation between two electrodes results in a capacitance change, which is then converted to a voltage using a MS3110 capacitive readout IC from *Irvine Sensors Corp* (Irvine Sensors 2009). Figure 6 shows the functional block diagram of the MS3110 capacitive readout IC. The MS3110 senses the change in capacitance between two capacitors and provides an output voltage proportional to that change. The capacitors, C1in and C2in form an external balanced pair. The output voltage of the MS3110 is given as (Irvine Sensors 2009)

$$V_O = Gain \times V2P25 \times 1.14 \times \frac{\{(C2in + C2) - (C1in + C1)\}}{C_F} + 0.5\,V, \quad (7)$$

where $V_O$ is the output voltage, *Gain* is fixed to 2 in this experiment, $V2P25 = 2.25$ V, $C_F$ is selected to optimize for input sense capacitance range, $C_F \geq 1.5$ pF. $C1in$ and $C2in$ are capacitance values from the fabricated micro-sensors. The capacitance of the resonating device is $C2in$ and that of the device on the anti-vibration table is $C1in$. $C1$ and $C2$ are programmable values. When $C2 = C1$, $\Delta C = (C2in - C1in)$. Therefore, $C2in$ and $C1in$ are expressed as $C2in = \frac{\varepsilon_0 A}{2}\left\{\frac{1}{(d-x)} + \frac{1}{(d+x)}\right\}$ and $C1in = C_0$ of (6), respectively.

Damping is one of the main significant loss mechanisms for the micro-resonator operating in air. For the moving direction perpendicular to the plane of two electrodes, the squeeze damping is dominant and thus substantially affects the system frequency response as well as the quality factor. For a rectangular plate with length $l$ and height $h$, where $l >> h$, the coefficient of damping force between the moving electrode and the fixed one is given by (Griffin et al. 1966)

$$D = \mu_{eff} \cdot l \cdot \left(\frac{h}{d}\right)^3, \quad (8)$$

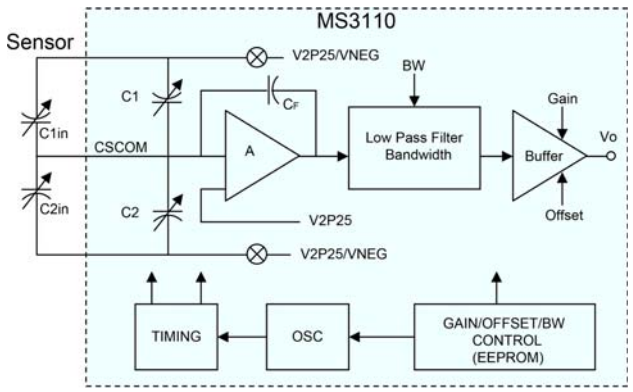


**Fig. 6** Functional block diagram of MS3110 [8]

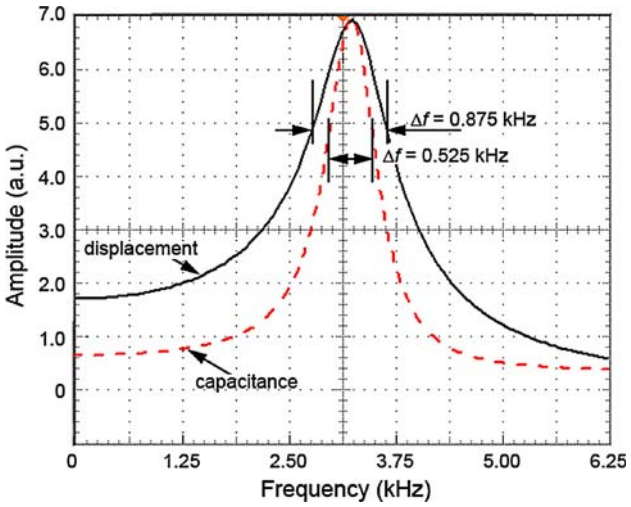


**Fig. 7** Simulated frequency responses of displacement and capacitance changes for 3.3 kHz micro-resonator. The 3 dB bandwidths are 0.875 and 0.525 kHz, respectively

where $\mu_{eff}$ is the effective fluid viscosity coefficient and $d$ is the gap between two plates or air film thickness. Using our device characteristics, the damping coefficient is $6.93 \times 10^{-4}$ kg/s at atmospheric pressure and room temperature.

The frequency responses of the resonator displacement and the capacitance change shown in Fig. 7 are calculated using the values of the simulated damping coefficient, the spring constant and the effective mass. Due to the non-linear behaviour between displacement and capacitance, the 3 dB bandwidth of capacitance change is 0.525 kHz while that of the displacement shows 0.875 kHz, resulting in different quality factors. Mechanical quality factor $Q$ is a very important quantity to identify the system. According to the simulations, the quality factor for the displacement graph is 3.8 while that of capacitance is 6.3 representing a relatively high selectivity and sensitivity.

Experiments validate our approach using microfabricated prototypes. The change in distance between two electrodes causes a capacitance change, which is then converted to a voltage. The device frequency characteristic measured at atmospheric pressure is presented in Fig. 8. The filter has a center frequency of about 3.3 kHz corresponding to the under-damped response. The 3 dB bandwidth is of 0.562 kHz and the quality factor $Q$ extracted from this plot is 5.9, which are in good agreement with the simulation result. The value of $Q$ shows that the fabricated device is quite adequate for sensing frequency of mechanical structure, whose resonant frequency is around 3.3 kHz.

Although the narrow bandwidth provides the high selectivity, it limits the operating range of the system. For certain applications, a wider bandwidth is necessary which

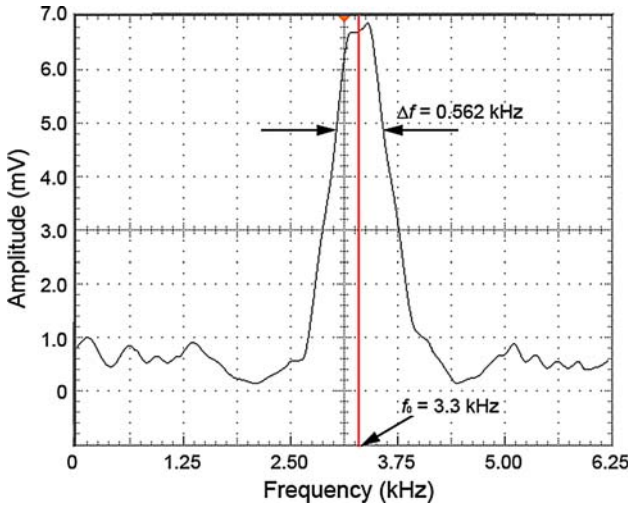


**Fig. 8** Frequency response of the microfabricated 3.3 kHz micro-resonator at atmospheric pressure. The 3 dB bandwidth is 0.562 kHz

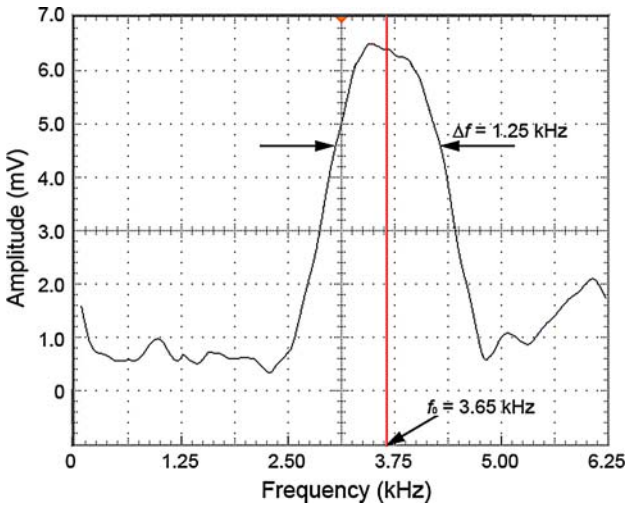


**Fig. 9** Frequency response of the microfabricated 3.3 kHz micro-resonator after adding a 3.9 kHz micro-resonator at atmospheric pressure. The 3 dB bandwidth is 1.25 kHz

increases the monitoring range. However, at a particular resonant frequency, if the bandwidth is wide or quality factor is a small value, the filter has poor selectivity and sensitivity. In this experiment, in order to increase the bandwidth keeping the same sensitivity, another resonator with a 3.9 kHz resonant frequency is placed in parallel to the 3.3 kHz resonator. Figure 9 shows the measured transmission spectrum for the parallel-resonator filter. The measurement is made at atmospheric pressure and the bandwidth of this filter is 1.25 kHz. It demonstrates the MEMS capacitive bandpass filter arrays with different resonant frequencies effectively increase the bandwidth for wider monitoring range.

The quality factor can be enhanced by reducing the damping force by a proper vacuum packaging process since the effective viscosity $\mu_{eff}$ of (8) is a function of pressure and air film width (Veijola et al. 1998):

$$\mu_{eff} = \frac{\mu}{1 + 9.638K_n^{1.159}}, \tag{9}$$

where $\mu$ is the viscosity coefficient of fluid. $K_n$ is Knudsen number defined as the ratio between the mean free path $\lambda$ and the air film thickness $d$ (Gad-et-Hak 1999):

$$K_n = \frac{\lambda}{d} = \frac{kT}{\sqrt{2}\pi\sigma^2 P \cdot d}. \tag{10}$$

Here, $P$ is pressure, $k$ is the Boltzmann constant, $T$ is temperature, and $\sigma$ is the molecular diameter. The value of $K_n$ determines the degree of rarefaction of the air and the validity of the continuous flow assumption. Gas flow regimes are classified given as follows: continuum flow for $K_n \leq 0.001$, slip flow for $0.001 \leq K_n \leq 0.1$, transition flow for $0.1 \leq K_n \leq 10$, and free molecular flow for $K_n > 10$. For $K_n > 10$, the mean free path length of gas is not negligible compared with the film thickness. Hence, the damping coefficient $D$ is tremendously reduced. Since the mechanical quality factor $Q$ is inversely proportional to the value of $D$, for a pressure much lower than an atmospheric pressure, much higher $Q$'s on the order of hundreds or thousands can be achieved, which will provide very high selectivity and high sensitivity.

## 5 Conclusions

In this paper, a highly selective MEMS bandpass filter is introduced and proposed using a resonant frequency sensitive sensing scheme. By means of utilization of resonant frequency of the micro-resonator, the proposed technique is able to detect input frequency of the monitored structure using small actuation force. Hence, the proposed MEMS bandpass filter offers both high sensitivity and selectivity and is a good candidate for vibration based sensing applications such as a structural health monitoring system. The micro-resonator is fabricated with a one-mask bulk silicon micromachining process on a SOI wafer resulting in resonant frequency of 3.3 kHz with 0.562 kHz of 3 dB bandwidth. The bandwidth is also increased by two resonators with different resonant frequencies. The parallel-resonator effectively increases the 3 dB bandwidth up to 1.25 kHz while keeping the same sensitivity. It shows for given applications and specifications, the resonant frequency and bandwidth of the sensors can be simply chosen by changing geometry of the mechanical structures and adding more sensors in parallel.

**Acknowledgment** The authors greatly acknowledge discussions with Dr. Patrice Masson and Dr. Philippe Micheau from Université de

Sherbrooke. This work was supported in part by CRIAQ (Consortium for Research and Innovation in Aerospace in Quebec).

## References

Gad-et-Hak M (1999) The fluid mechanics of micro devices—the freeman scholar lecture. J Fluids Eng 121:5–32. doi:10.1115/1.2822013

Griffin WS, Richardson HH, Yamanami S (1966) A study of fluid squeeze-film damping. ASME J Basic Eng 88:451–456

Irvine Sensors (2009) MS3110 Universal Capacitive Readout™ IC. Accessed 12 March, 2009 from http://www.irvine-sensors.com/pdf/MS3110%20Datasheet%20USE.pdf

Johnson RA (1983) Mechanical filters in electronics. Wiley, New York

Li G, Li Z, Wang C, Hao Y, Li T, Zhang D, Wu G (2001) Design and fabrication of a highly symmetrical capacitive triaxial accelerometer. J Micromech Microeng 11:48–54. doi:10.1088/0960-1317/11/1/308

Ludtke O, Biefeld V, Buhrdorf A, Binder J (2000) Laterally driven accelerometer fabricated in single crystalline silicon. Sens Actuators A Phys 82:149–154. doi:10.1016/S0924-4247(99)00328-3

Reithmuller W, Benecke W, Schnakenberg U, Wagner B (1992) A smart accelerometer with on-chip electronics fabricated by a commercial CMOS process. Sens Actuators A Phys 31:121–124. doi:10.1016/0924-4247(92)80090-P

Seidel H, Fritsch U, Gottinger R, Schalk J (1995) A piezoresistive silicon accelerometer with monolithically integrated CMOS-circuitry. Tech. Dig. 8th Int. Conf. Solid-State Sensors and Actuators (Transducers' 95):597–600

Song IH, Ajmera PK (2009) A laterally movable gate field effect transistor. IEEE/ASME J Microelectromech Syst 18:208–216. doi:10.1109/JMEMS.2008.2008623

Veijola T, Kuisma H, Lahdenpera J, Ryhanen T (1998) Equivalent-circuit model of the squeezed gas film in a silicon accelerometer. Sens Actuators A Phys 48:239–248. doi:10.1016/0924-4247(95)00995-7

Yeh C, Najafi K (1997) A low-voltage tunneling-based silicon micro-accelerometer. IEEE Trans Electron Dev 44:1875–1882. doi:10.1109/16.641355